Submitted: 11 June, 2025 Accepted: 21 August, 2025 Published: 30 May, 2026 DOI:10.22514/jomh.2026.042

ORIGINAL RESEARCH

JOMH Journal of Men's Health

Plasma proteome-based integrated mendelian randomization and multi-omics analysis identifies potential diagnostic biomarkers and therapeutic targets for prostate cancer

Hua Xiang[1], Qian Liu[1,*]

[1]Department of Urology, Changde Hospital, Xiangya School of Medicine, Central South University (The First People's Hospital of Changde City), 415000 Changde, Hunan, China

***Correspondence**
2024141480190@stu.scu.edu.cn
(Qian Liu)

Abstract

Background: Prostate cancer (PCa) is a major cause of cancer-related deaths in men, with challenges in early detection and effective treatment. Plasma proteins have emerged as promising diagnostic biomarkers and therapeutic due to their accessibility and reflection of tumor-related systemic changes. **Methods**: We performed a Mendelian randomization (MR) analysis to identify causal plasma proteins associated with PCa. Multi-omics data, including bulk RNA sequencing (RNA-seq), single-cell RNA sequencing (scRNA-seq), and spatial transcriptomics, were integrated to explore molecular, cellular, and spatial expression patterns. Functional enrichment analysis (Gene Ontology (GO)/Kyoto Encyclopedia of Genes and Genomes (KEGG)), diagnostic receiver operating characteristic (ROC) analysis, immune infiltration analysis, and molecular docking were conducted to elucidate their biological roles and therapeutic potential. **Results**: MR analysis identified 66 plasma proteins associated with PCa, highlighting their roles in extracellular matrix remodeling and inflammation. Multi-omics integration revealed four key biomarkers (transforming growth factor beta 3 (TGFB3), insulin-like growth factor binding protein 6 (IGFBP6), Golgi membrane protein 1 (GOLM1), and serpin family F member 1 (SERPINF1)) with distinct spatial expression patterns and links to tumor progression and immune modulation. TGFB3, IGFBP6, and SERPINF1 correlated positively with immune infiltration and checkpoints, while GOLM1 showed negative correlations. A combined diagnostic model achieved excellent accuracy (area under the curve (AUC) = 0.911). Functional enrichment connected these factors to pathways like Suppressor of Mothers Against Decapentaplegic (SMAD) signaling and Wingless/Integrated (Wnt) signaling. Small molecule screening and molecular docking identified diethylstilbestrol as a therapeutic candidate targeting TGFB3 and IGFBP6. **Conclusions**: Our findings provide novel insights into the molecular mechanisms of PCa and highlight promising diagnostic and therapeutic targets. Further experimental validation and clinical studies are needed to confirm these results and assess their translational potential.

Keywords

Prostate cancer; Plasma proteome; Mendelian randomization; Multi-omics integration; Diagnostic biomarkers; Therapeutic targets

1. Introduction

Prostate cancer (PCa) is one of the most prevalent malignancies among men worldwide, ranking as the second leading cause of cancer-related deaths in this population [1]. According to global cancer statistics, PCa accounts for over 1.4 million new cases and approximately 375,000 deaths annually [2]. The disease burden is particularly high in developed countries, where aging populations and lifestyle factors contribute to its increasing incidence. Despite advances in diagnostic and therapeutic strategies, challenges remain in achieving early detection and effective treatment. This underscores the urgent need to identify reliable diagnostic biomarkers and therapeutic targets to improve clinical outcomes for PCa patients [3].

In recent years, plasma proteins have emerged as promising candidates for diagnostic and therapeutic applications in cancer [4–6]. Their accessibility through minimally invasive procedures, such as blood sampling, makes them ideal for clinical use. Moreover, plasma proteins can reflect systemic changes associated with tumorigenesis, including alterations in

the tumor microenvironment (TME), immune responses, and metabolic processes [7–9]. These unique advantages position plasma proteins as valuable tools for identifying causal factors and actionable targets in PCa.

Mendelian randomization (MR) analysis has gained traction as a robust approach for uncovering causal relationships between exposures and outcomes, leveraging genetic variants as instrumental variables to infer causality [10]. By applying MR to plasma proteome data, researchers can identify plasma proteins that play a direct role in PCa development, distinguishing causal factors from mere associations. This approach not only enhances our understanding of PCa pathogenesis but also facilitates the prioritization of plasma proteins for further investigation as diagnostic biomarkers or therapeutic targets.

The advent of multi-omics technologies has revolutionized cancer research, offering unprecedented insights into the molecular and cellular landscapes of tumors [11]. Integrating bulk RNA sequencing (bulk RNA-seq), single-cell RNA sequencing (scRNA-seq), and spatial transcriptomics (ST) provides a comprehensive understanding of PCa at multiple levels [12]. Bulk RNA-seq enables the identification of differentially expressed genes (DEGs) between tumor and normal tissues, while scRNA-seq uncovers cell type-specific gene expression profiles and intercellular interactions [13]. ST further adds spatial resolution, revealing the spatial organization and heterogeneity of gene expression within the tumor microenvironment [14]. Combining these multi-omics approaches with MR analysis allows for the identification of causal plasma proteins whose gene-level expression is significantly altered in PCa, providing a holistic view of their roles in disease progression.

In this study, we employed an integrated approach combining MR analysis and multi-omics data to identify potential diagnostic biomarkers and therapeutic targets for PCa. By leveraging plasma proteome data and integrating bulk RNA-seq, scRNA-seq, and ST datasets, we aimed to uncover causal plasma proteins associated with PCa and validate their expression patterns at both the transcriptional and spatial levels. Our findings provide novel insights into the molecular mechanisms underlying PCa and highlight promising plasma protein candidates for clinical translation in diagnosis and treatment.

2. Methods

2.1 Data mining and collection

We obtained protein quantitative trait loci (pQTL) data from a study conducted by Ferkingstad *et al.* [15] using deCODE genetics (https://www.decode.com/summarydata/). The pQTL data satisfied the following criteria: (a) genome-wide significant associations ($p < 5 \times 10^{-8}$) and (b) independent associations (linkage disequilibrium (LD) clumping $r^2 < 0.001$). Summary statistics for PCa were acquired from the Integrative Epidemiology Unit (IEU) Open Genome-Wide Association Studies (GWAS) project (https://gwas.mrcieu.ac.uk/), with the analytical cohort (GWAS ID: ebi-a-GCST90018905, European) comprising 11,599 PCa cases and 199,628 controls, encompassing 211,227 single nucleotide polymorphisms (SNPs).

Besides, two bulk RNA-seq datasets (GSE200879 and GSE46602), a single-cell transcriptomic dataset (GSE193337), and a spatial transcriptomic dataset (GSE278936), containing human prostate cancer and normal prostate tissues, were retrieved from the Gene Expression Omnibus (GEO) database (http://www.ncbi.nlm.nih.gov/geo). The annotation information provided on the respective platforms was used as a reference for mapping corresponding gene symbols. Clinical information of patients with PCa and their corresponding mRNA expression data were downloaded from The Cancer Genome Atlas (TCGA) website (https://cancergenome.nih.gov/).

2.2 Mendelian randomization analysis

A bidirectional two-sample Mendelian randomization (MR) approach was employed to investigate the causal relationship between the human plasma proteome and prostate cancer (PCa). In this study, the plasma proteome was considered the exposure, and PCa was treated as the outcome, aiming to identify their potential roles as protective or risk-enhancing factors in PCa development.

Five analytical methods were applied to ensure robust causal inference, including inverse variance-weighted (IVW), MR-Egger, weighted median, simple mode, and weighted mode. IVW served as the primary method, while the other four methods were used as supplementary tools to validate the results. The IVW method combines Wald estimates from individual SNPs using a meta-analytic framework to generate an overall causal estimate, represented by the slope of the weighted regression of outcome effects on exposure effects [16]. The MR-Egger method was applied to assess horizontal pleiotropy, while the weighted median approach, recognized for its robustness in smaller datasets, served as a complementary method to enhance the reliability of the IVW and MR-Egger analyses [17]. The "TwoSampleMR" [18] and "MR-Pleiotropy RESidual Sum and Outlier (PRESSO)" [19] R packages were utilized in R (version 4.4.2) to perform the MR analyses and evaluate potential pleiotropy or other biases.

2.3 Sensitivity analysis and direction validation in MR

The MR-Egger intercept test [20] was applied to detect horizontal pleiotropy, with a statistically significant intercept indicating its presence. Cochran's Q test [21] was used to evaluate SNP heterogeneity, and a significant Q statistic reflected the presence of heterogeneity. Sensitivity analysis was performed using the leave-one-out method, systematically excluding each SNP to assess the robustness of the results. Consistent MR estimates after the exclusion of individual SNPs demonstrated the reliability of the findings. A p-value < 0.05 was considered statistically significant. In the absence of pleiotropy and heterogeneity, the Inverse Variance-Weighted method was deemed valid.

2.4 Bulk RNA-seq data processing

Data normalization was performed using the limma package [22] to correct batch effects, with raw expression matrices log2-transformed and normalized via the NormalizeBe-

tweenArrays function. Principal component analysis (PCA) confirmed the removal of batch effects. The limma package was used to identify differentially expressed genes (DEGs) with $|\log FC| > 0.585$ and an adjusted p-value < 0.05. Volcano plots and heatmaps of the top upregulated and downregulated genes were respectively generated using ggplot2 [23] and pheatmap packages [24], to visualize transcriptional changes.

2.5 Single-cell RNA-seq data processing

The single-cell RNA sequencing data were processed using standard workflows [25], including normalization, dimensionality reduction, clustering, cell type annotation, and intercellular communication analysis. A Seurat object was created, and low-quality cells ($\leq$50 feature genes or $\geq$15% mitochondrial gene content) were removed. Data normalization was performed with the LogNormalize method (scale factor: 10,000), and highly variable genes were identified using variance-stabilizing transformation (VST). PCA was used for dimensionality reduction, with the top 20 components selected. Batch effects were corrected using the Harmony algorithm, and t-distributed stochastic neighbor embedding (t-SNE) was applied for visualizing cell distribution patterns.

Clustering analysis was conducted using the Louvain algorithm on shared nearest neighbor (SNN) graphs with a resolution of 0.6. Marker genes were identified through differential expression analysis (log2 FC >1, adjusted p-value < 0.05) and used to annotate cell clusters based on their expression patterns. Cell type annotation was further refined with the SingleR [26] tool and reference databases (*e.g.*, HumanPrimaryCellAtlas and BlueprintEncode), identifying major cell types including cluster of differentiation (CD)4+ T cells, CD8+ T cells, B cells, monocytes, macrophages, fibroblasts, and endothelial cells. Manual curation and marker gene validation were conducted to ensure accurate annotation.

2.6 Spatial transcriptomic data processing

Spatial transcriptomic (ST) data were processed and analyzed to explore spatially resolved gene expression patterns [27]. The raw data were normalized and corrected using the SCTransform method, followed by dimensionality reduction (PCA), clustering, and visualization using Uniform Manifold Approximation and Projection (UMAP). The FindAllMarkers and FindMarkers functions, implemented in the Seurat R package, were used to identify DEGs derived from spatial transcriptomic data (ST-DEGs), which provide insights into spatially localized gene expression patterns and the molecular heterogeneity across tissue regions.

2.7 Multiple intercellular analysis

To investigate the spatial organization of cell types and their interactions within the tissue, we employed Multiple Intercellular Analysis (MIA), which integrates scRNA-seq data with ST data. Although ST data provide spatial resolution, they lack the cellular resolution of scRNA-seq. MIA overcomes this limitation by mapping scRNA-seq-derived cell type information onto the spatial context of ST data through shared gene expression profiles. This approach enables the identification of spatially resolved cell types, their functional states, and potential intercellular communication networks, providing a comprehensive view of the tissue microenvironment.

2.8 Functional enrichment analysis and PPI network construction

Gene Ontology (GO) analysis is a widely used method for annotating genes and their products by categorizing them into three main domains, including biological processes (BP), cellular components (CC), and molecular functions (MF). The Kyoto Encyclopedia of Genes and Genomes (KEGG) serves as a comprehensive resource that systematically analyzes biological pathways, integrating genomic, chemical, and functional information to elucidate molecular interactions and cellular processes. In this study, we utilized the DOSE (v3.22.0) [28] and clusterProfiler [29] (v4.4.4) packages in R (v4.2.1) to explore the biological relevance of the gene set and conduct pathway enrichment analyses. Furthermore, the enrichplot and ggplot2 packages were employed to generate high-quality visualizations of the results. The protein-protein interaction (PPI) network was constructed using the GeneMANIA [30] prediction server (http://www.genemania.org/).

2.9 Immune profiling analysis

The association between gene expression and the tumor immune microenvironment was analyzed using bulk RNA-seq data obtained from the TCGA-prostate adenocarcinoma (PRAD) cohort. Spearman correlation analysis was employed to assess the relationship between gene expression and immune cell infiltration levels, as well as the immune infiltration matrix data. Samples were stratified into high- and low-expression groups based on the median expression level of key biomarkers. Immune infiltration levels were quantified using the single-sample gene set enrichment analysis (ssGSEA) algorithm implemented in the Gene Set Variation Analysis (GSVA) package [31] (v1.46.0), with immune cell markers for 24 distinct immune cell types. The ggplot2 package was used to visualize the results.

2.10 Small molecule screening and molecular docking analysis

The relationships between small molecules and target proteins were obtained from the DsigDB [32] database (https://dsigdb.tanlab.org/). Network Venn diagrams were visualized using R software (v4.2.1) with the igraph (v1.4.1), ggraph (v2.1.0), and ggplot2 (v3.4.4) packages. Protein structure data were retrieved from the PDB database [33] (https://www.rcsb.org/), and the three-dimensional structures of small molecules were downloaded from the PubChem database [34] (https://pubchem.ncbi.nlm.nih.gov/). Molecular docking was performed using the CB-dock2 [35] online tool (https://cadd.labshare.cn/cb-dock2/index.php) to predict the binding modes between small molecules and target proteins.

2.11 Statistical analysis

Continuous variables were expressed as mean $\pm$ standard deviation (SD). For comparisons between two independent groups,

the Student's *t*-test was applied for data following a normal distribution, while the Wilcoxon rank-sum test was used for non-normally distributed data. Paired samples were analyzed using either the paired *t*-test or the Wilcoxon signed-rank test, based on the distribution of the data. Correlations between variables were assessed using the Pearson correlation coefficient. Diagnostic performance was evaluated using receiver operating characteristic (ROC) curves, and the area under the curve (AUC) was calculated to quantify accuracy. A significance threshold of $p < 0.05$ was applied for all statistical tests.

3. Results

3.1 Flow chart and related data information

The workflow of this study design is illustrated in Fig. 1. The characteristics of each enrolled PCa dataset downloaded from GEO database are summarized in Table 1, and the detailed information is provided in **Supplementary Table 1**.

3.2 Identification of PCa-associated plasma proteins through MR analysis

After removing SNPs with insufficient instrument strength (*F*-statistic < 10), a total of 31,315 SNPs associated with 3457 plasma proteins were identified (**Supplementary Table 2**). To ensure the robustness of the instrumental variables (IVs), the distribution of *F*-statistics was assessed, ranging from 29.71 to 57,932.93, with a median of 54.75 and a mean of 184.27, demonstrating strong instrument strength across all included SNPs (**Supplementary Fig. 1**). MR analysis using these IVs identified 66 plasma proteins with IVW *p*-values < 0.05 (**Supplementary Table 3**). The circular plot shows the *p*-value distributions of plasma proteins across five MR methods (Fig. 2a). The volcano plot (Fig. 2b) highlights the regression coefficients (Beta values) and −log10(*p*-values) for these PCa-associated plasma proteins (PCa-PP), with significant proteins such as Collagen Type III Alpha 1 Chain (COL3A1) and Interleukin 1 Receptor Like 2 (IL1RL2) exhibiting significant associations. The Manhattan plot (Fig. 2c) further illustrates the genomic distribution of significant proteins across chromosomes, emphasizing the importance of COL3A1 and IL1RL2 in the causal relationship with PCa.

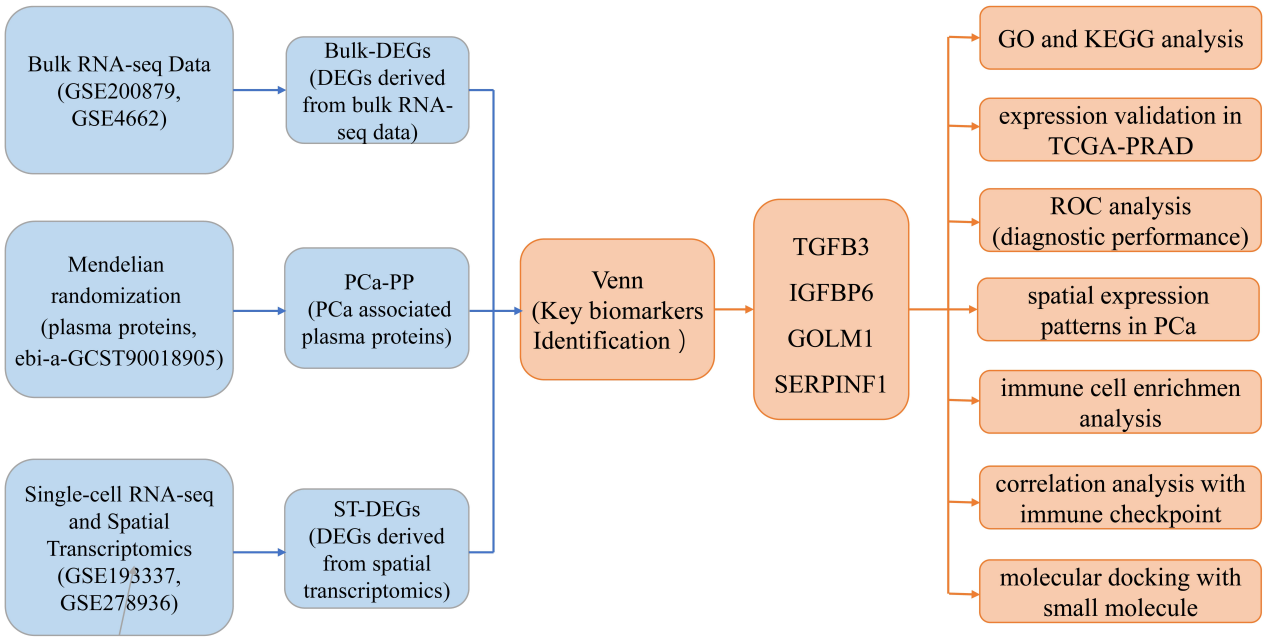

FIGURE 1. The workflow of this study design. DEGs, differentially expressed genes; GO, Gene Ontology; GOLM1, Golgi membrane protein 1; IGFBP6, insulin-like growth factor binding protein 6; PCa, Prostate cancer; PRAD, prostate adenocarcinoma; ROC, receiver operating characteristic; SERPINF1, serpin family F member 1; ST, spatial transcriptomic; TCGA, The Cancer Genome Atlas; TGFB3, transforming growth factor beta 3; KEGG, Kyoto Encyclopedia of Genes and Genomes.

TABLE 1. The characteristics of each enrolled prostate cancer dataset downloaded from GEO database.

Record	Type	Platform	Normal	Tumor	Country
GSE46602	Bulk RNA-seq	GPL570	14	36	Denmark
GSE200879	Bulk RNA-seq	GPL32170	9	128	France
GSE193337	Single-cell RNA-seq	GPL20301	4	4	Austria
GSE278936	Spatial transcriptomics	GPL24676	4	17	Finland

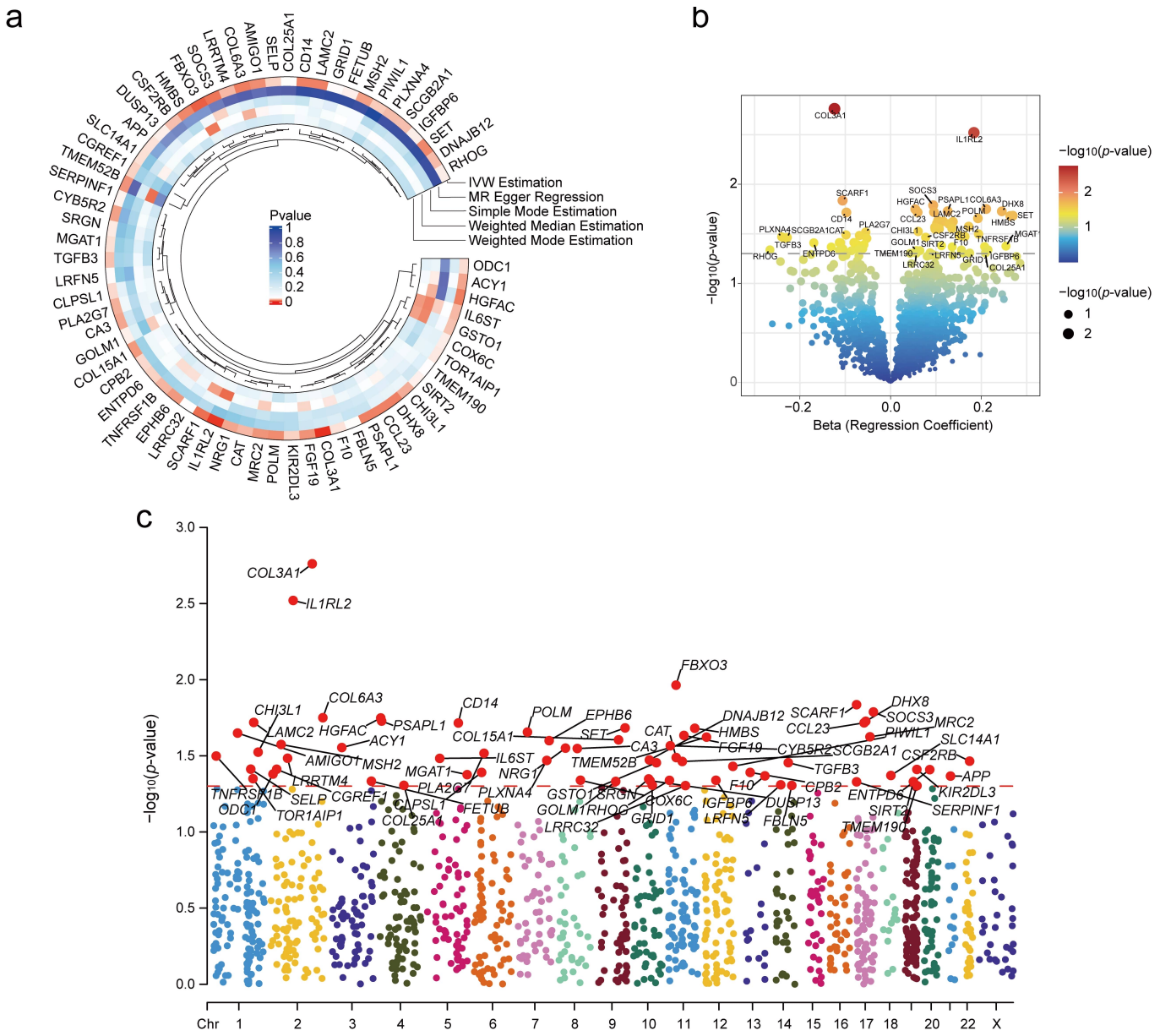

FIGURE 2. Results of MR Analysis. (a) Circular plot showing the *p*-value distribution of plasma proteins across five MR methods. Each row represents a protein, and each column represents a method. (b) Volcano plot illustrating the distribution of Beta coefficients and −log10(*p*-values) for plasma proteins. (c) Manhattan plot displaying the genomic distribution of significant plasma proteins. Beta, Regression Coefficient; IVW Estimation, Inverse Variance Weighted Estimation; MR, Mendelian Randomization; Chr, Chromosome.

3.3 Identification of DEGs based on bulk RNA-seq data

After normalizing gene expression across datasets (Fig. 3a,b), 966 DEGs derived from bulk RNA-seq data (bulk-DEGs) were identified, including 335 upregulated and 631 downregulated genes (Fig. 3c, **Supplementary Table 4**). The top 20 upregulated and downregulated genes ranked by fold change were displayed in a heatmap, which showed significant differences in gene expression patterns between PCa and normal prostate tissue samples (Fig. 3d).

3.4 Integration of single-cell RNA-seq and spatial transcriptomics

Single-cell RNA sequencing (scRNA-seq) identified 25 clusters, representing 11 major cell types, including immune cells (CD4+ T cells, CD8+ T cells, macrophages), fibroblasts, and epithelial cells (Fig. 4a). Differences in cell distribution were observed between normal and tumor samples. In tumor samples, CD4+ and CD8+ T cells exhibited a more localized and concentrated distribution compared to normal tissues, whereas epithelial and fibroblast cells showed a more dispersed distribution (Fig. 4b). Spatial transcriptomics (ST) analysis further identified 24 spatially resolved clusters, underscoring the cellular heterogeneity across samples (Fig. 4c). The DEGs associated with spatial transcriptomics data (ST-DEGs) between

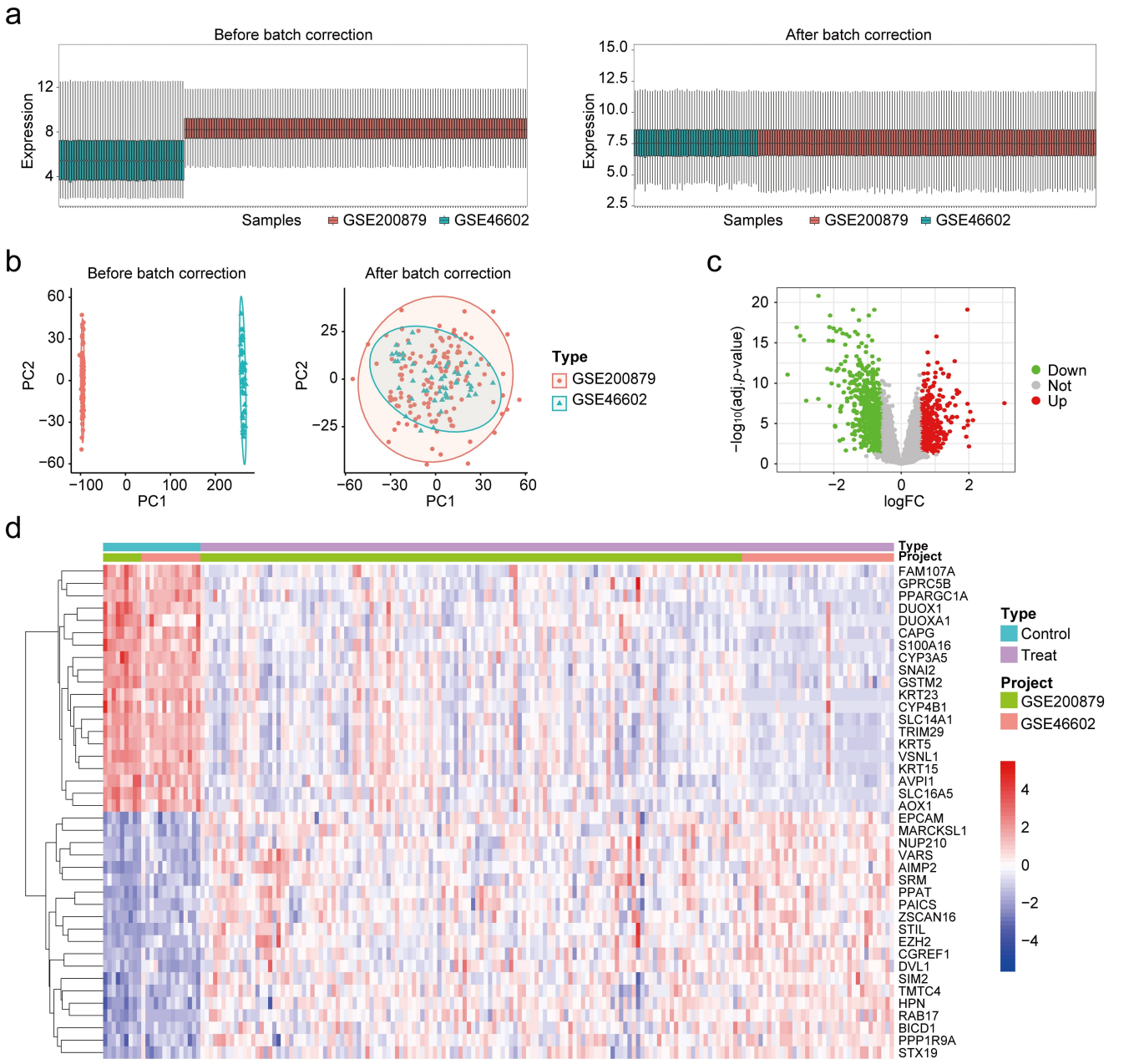

FIGURE 3. Identification of DEGs based on bulk RNA-seq data. (a) Batch effect correction across datasets. (b) Principal component analysis (PCA) before and after batch effect correction. (c) Volcano plot of DEGs. Upregulated genes are shown in red, downregulated genes in green, and non-significant genes in gray. (d) Heatmap of the top 20 upregulated and downregulated DEGs. Red and blue indicate high and low expression levels by logFC, respectively.

normal and tumor samples were identified for further analysis (**Supplementary Table 5**). Annotation of major clusters using MIA revealed that clusters 6 and 24 were significantly enriched with immune cells, including CD4+ T cells, CD8+ T cells, macrophages, and monocytes. In contrast, other clusters showed limited immune cell types, suggesting a distinct immune cell aggregation pattern in these clusters (Fig. 4d, **Supplementary Table 6**). Additionally, spatial visualization of selected normal and tumor sample slices demonstrated a marked increase in the absolute abundance of clusters 6, 24, and 23 in tumor samples, whereas clusters 7, 9, and 11 exhibited a relatively higher proportion in normal samples (Fig. 4e). This pattern indicates a significant enrichment of immune cell-related clusters in the tumor microenvironment, while stromal cell-related clusters are more abundant in normal tissue.

3.5 GO and KEGG analysis of PCa-PP, Bulk-DEGs, and ST-DEGs

The GO and KEGG enrichment analyses provided insights into the biological processes and pathways associated with PCa across different datasets. For PCa-PP, significant enrichment was observed in terms related to extracellular matrix dynamics, including extracellular matrix structural constituents, collagen-containing extracellular matrix, and processes like wound healing and regulation of inflammatory responses (Fig. 5a, **Supplementary Table 7**). These results highlight the role of extracellular remodeling and immune regulation in PCa pro-

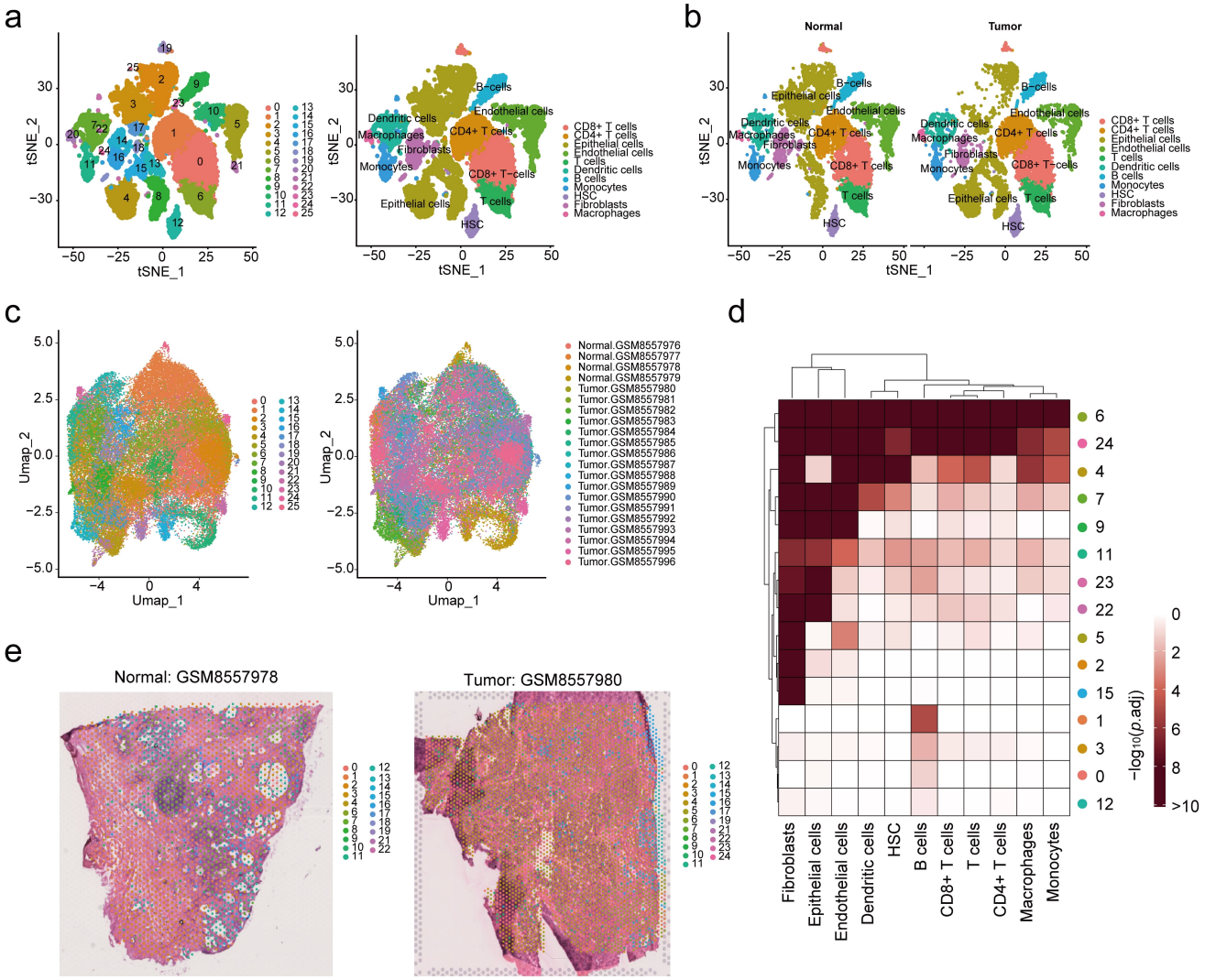

FIGURE 4. Integration of single-cell RNA-seq and spatial transcriptomics. (a) Identification of 25 distinct cell clusters and 11 major cell types from the scRNA-seq dataset GSE193337. (b) Comparison of cell distribution patterns between normal and tumor samples. (c) Spatial transcriptomics analysis identified 25 spatially resolved clusters from the ST dataset GSE278936, revealing cellular heterogeneity across samples. (d) Annotation of major clusters using MIA analysis. (e) Spatial visualization of normal and tumor sample slices.

gression. For Bulk-DEGs, pathways and biological functions such as glutathione metabolism, the phosphatidylinositol 3-kinase-protein kinase B (PI3K-Akt) signaling pathway, glycosaminoglycan binding, and epithelial cell proliferation were significantly enriched (Fig. 5b, **Supplementary Table 8**), reflecting alterations in metabolic processes, cell signaling, and extracellular matrix interactions in PCa. Finally, ST-DEGs revealed enrichment in functions such as complement and coagulation cascades, cell adhesion molecules, and extracellular matrix organization (Fig. 5c, **Supplementary Table 9**), emphasizing the importance of immune modulation, cell adhesion, and structural reorganization in the tumor microenvironment. These findings collectively underscore the critical roles of extracellular matrix remodeling, immune regulation, and metabolic shifts in PCa pathogenesis.

3.6 Key biomarkers identification and enrichment analysis

To identify key biomarkers associated with PCa progression, we integrated the results of PCa-PP and DEGs, identifying four key biomarkers, including TGFB3, IGFBP6, GOLM1, and SERPINF1 (Fig. 6a). A PPI network was constructed to visualize the interactions among these biomarkers and related proteins (Fig. 6b). Subsequently, GO and KEGG enrichment analyses were performed, and tumor progression-related terms were displayed in lollipop plots (Fig. 6c, **Supplementary Table 10**). The results showed involvement in epithelial to mesenchymal transition, SMAD signaling regulation, cytokine binding, extracellular matrix components, and pathways such as growth factor binding and the Wnt signaling pathway.

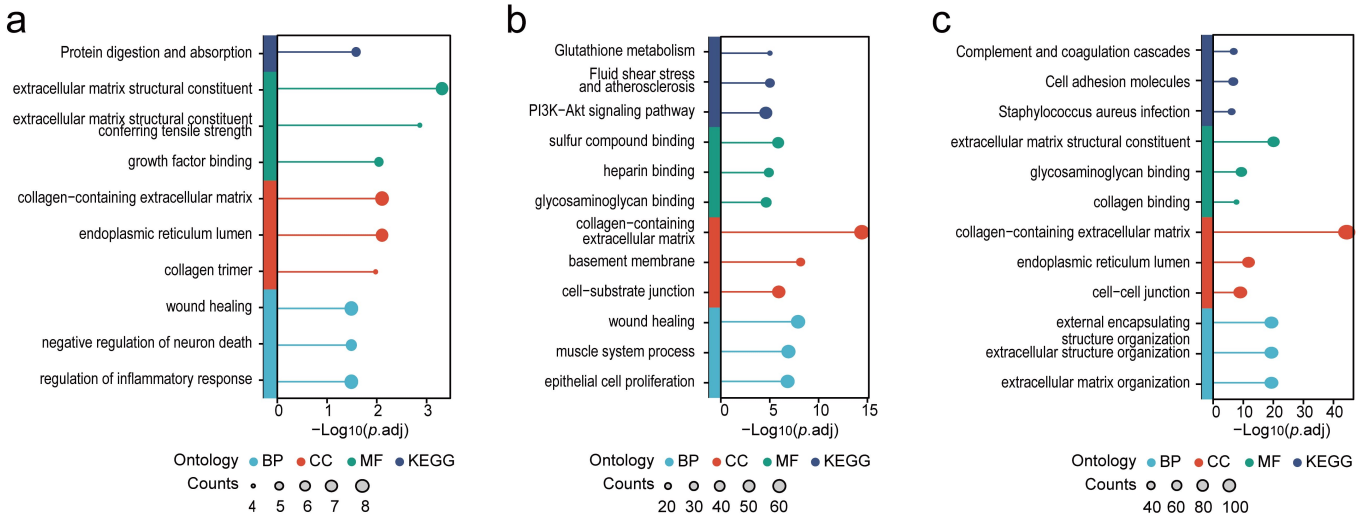

FIGURE 5. Results of GO and KEGG analysis. (a) GO and KEGG enrichment analysis of PCa-associated plasma proteins (PCa-PP), (b) DEGs derived from bulk RNA-seq data (bulk-DEGs), and (c) DEGs associated with spatial transcriptomics data (ST-DEGs). BP, biological processes; CC, cellular components; MF, molecular functions; KEGG, Kyoto Encyclopedia of Genes and Genomes; PI3K, Phosphatidylinositol 3-Kinase; Akt, Protein Kinase B.

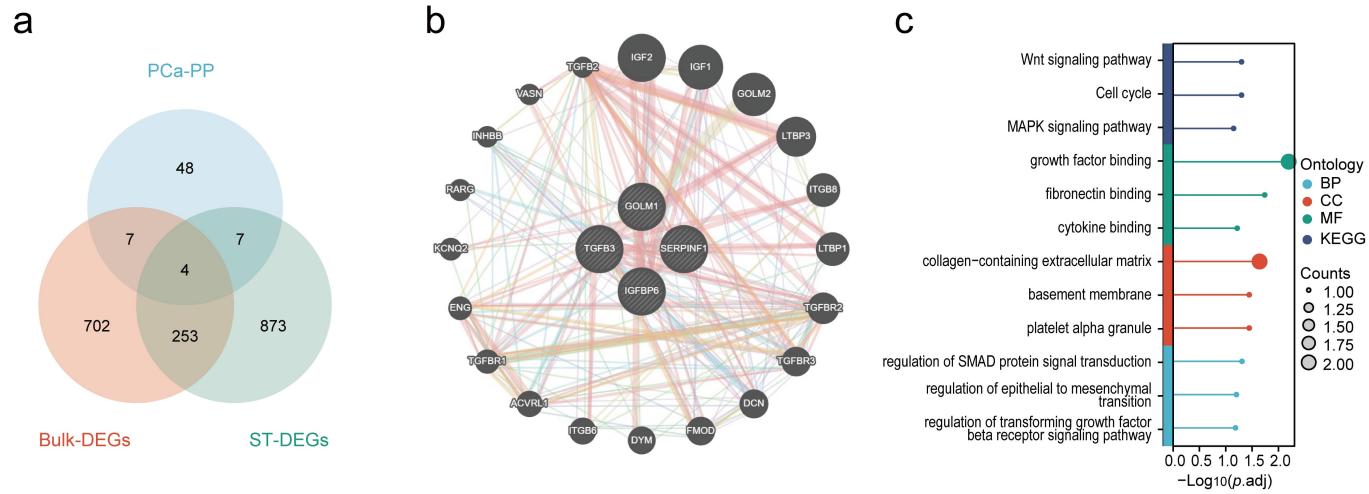

FIGURE 6. Key biomarkers identification and enrichment analysis. (a) Venn diagram integrating PCa-PP and DEGs to identify key biomarkers. (b) PPI network visualizing the interactions among the four key biomarkers and related proteins. (c) Results of GO and KEGG enrichment analyses of the key biomarkers, with tumor progression-related terms displayed. MAPK, mitogen-activated protein kinase; PCa-PP, prostate cancer-associated plasma proteins; ST, spatial transcriptomics; SMAD, mothers against decapentaplegic homolog; DEGs, differentially expressed genes.

3.7 Key biomarkers expression validation and diagnostic performance in PCa

The TCGA-PRAD cohort was analyzed to validate the expression patterns of the four key biomarkers in PCa. The results revealed that IGFBP6, TGFB3, and SERPINF1 were significantly downregulated in tumor tissues compared to normal tissues, whereas GOLM1 was upregulated (Fig. 7a). Paired sample analysis further confirmed these expression patterns with significant differences (Fig. 7b). ROC curve analysis demonstrated that GOLM1 exhibited the highest diagnostic performance (AUC = 0.859), followed by SERPINF1 (AUC = 0.762), TGFB3 (AUC = 0.728), and IGFBP6 (AUC = 0.706) (Fig. 7c). Furthermore, a diagnostic model combining the four factors achieved an AUC of 0.911 (95% CI: 0.869–0.953), indicating excellent diagnostic accuracy (Fig. 7d). External validation was performed using independent datasets GSE46602 and GSE200879 to assess the robustness and generalizability of the diagnostic model (Fig. 7e–h). The model achieved AUCs of 0.994 in GSE46602 and 0.974 in GSE200879, strongly supporting its high diagnostic performance and potential clinical utility.

3.8 Spatial expression patterns of key biomarkers in PCa

Spatial transcriptomics data were analyzed to further evaluate the expression patterns of the key biomarkers, revealing distinct regional differences between normal prostate and PCa tissues. The results demonstrated that TGFB3, IGFBP6, and

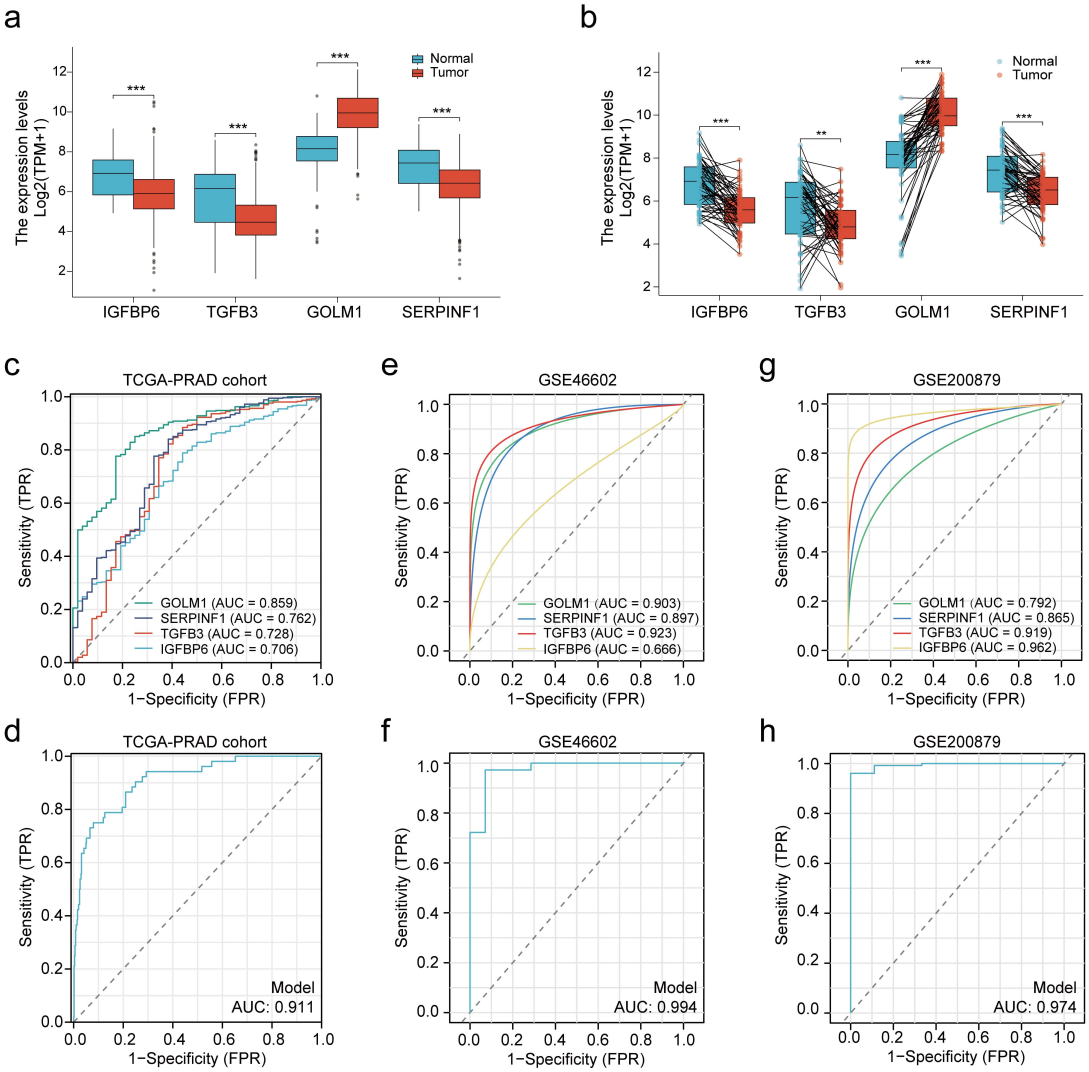

FIGURE 7. Key biomarkers expression validation and diagnostic performance in PCa. (a) Expression levels of key biomarkers in PCa and normal prostate tissues. (b) Paired sample analysis validating the differential expression of key biomarkers. Statistical significance is denoted by ** and *** for $p < 0.01$ and $p < 0.001$, respectively. (c) ROC curve analysis illustrating the diagnostic performance of individual key biomarker in TCGA-PRAD cohort. (d) A combined diagnostic model integrating the four key biomarkers in TCGA-PRAD cohort. (e) ROC curve analysis illustrating the diagnostic performance of individual key biomarker in the GSE46602. (f) A combined diagnostic model integrating the four key biomarkers in the GSE46602. (g) ROC curve analysis illustrating the diagnostic performance of individual key biomarker in the GSE200879. (h) A combined diagnostic model integrating the four key biomarkers in the GSE200879. TCGA, The Cancer Genome Atlas; AUC, area under the curve; TMP, Tumor Microenvironment Proteins; TRP, Tumor-Related Proteins; FRP, Fibrosis-Related Proteins; PRAD, Prostate Adenocarcinoma; IGFBP6, Insulin-Like Growth Factor Binding Protein 6; TGFB3, Transforming Growth Factor Beta 3; GOLM1, Golgi Membrane Protein 1; SERPINF1, Serpin Family F Member 1.

SERPINF1 were significantly downregulated in PCa tissues compared to normal tissues, while GOLM1 was notably upregulated (Fig. 8). This spatial visualization highlights the contrasting expression profiles of these factors and their potential roles in PCa progression.

3.9 Immune microenvironment characteristics of key biomarkers in PCa

Immune cell enrichment score analysis was performed to compare high and low expression groups of TGFB3, IGFBP6, GOLM1, and SERPINF1 (Fig. 9a–d), with their correlations to various immune cell types summarized in a heatmap (Fig. 9e). As shown, TGFB3 and IGFBP6 demonstrated positive correlations with most immune cell types, including T cells, B cells, macrophages, and dendritic cells, highlighting their roles in promoting immune cell infiltration. Similarly, SERPINF1 exhibited positive correlations with a broad range of immune cell types. In contrast, GOLM1 displayed significant negative correlations with specific immune cells, such as neutrophils, mast cells, and macrophages, suggesting its potential role in suppressing their infiltration. Furthermore, correlation analysis with immune checkpoint molecules revealed that TGFB3, IGFBP6, and SERPINF1 were strongly and positively correlated with checkpoint molecules such as PDCD1, CD274, and CTLA4, whereas GOLM1 showed significant negative corre-

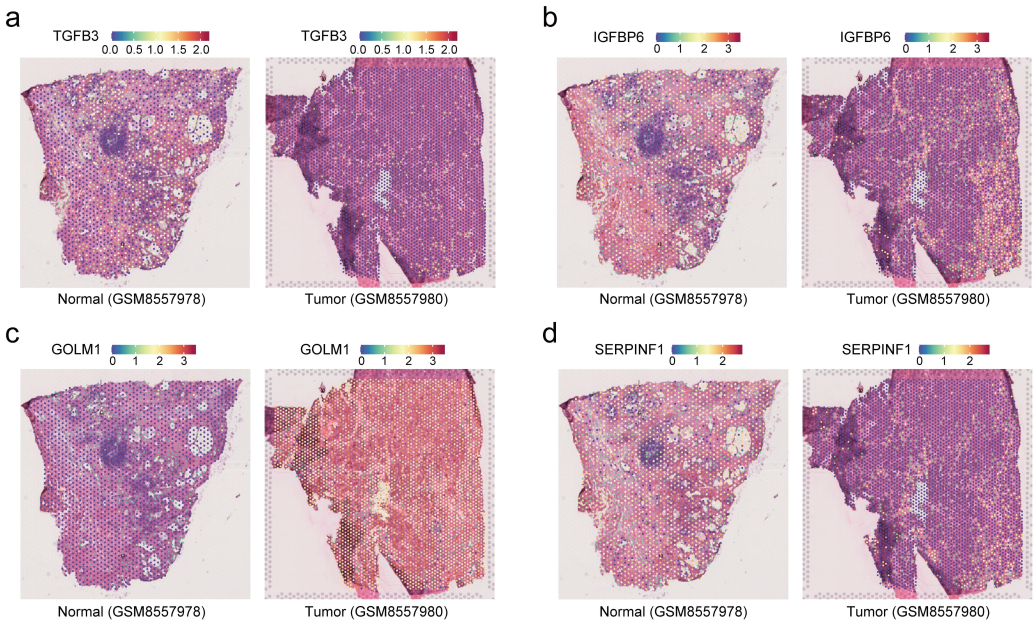

FIGURE 8. Spatial expression patterns of key biomarkers in PCa. The spatial transcriptomics data were analyzed to evaluate the expression patterns of (a) TGFB3, (b) IGFBP6, (c) GOLM1, (d) and SERPINF1 in normal prostate and PCa tissues. TGFB3, Transforming Growth Factor Beta 3; IGFBP6, Insulin-Like Growth Factor Binding Protein 6; GOLM1, Golgi Membrane Protein 1; SERPINF1, Serpin Family F Member 1.

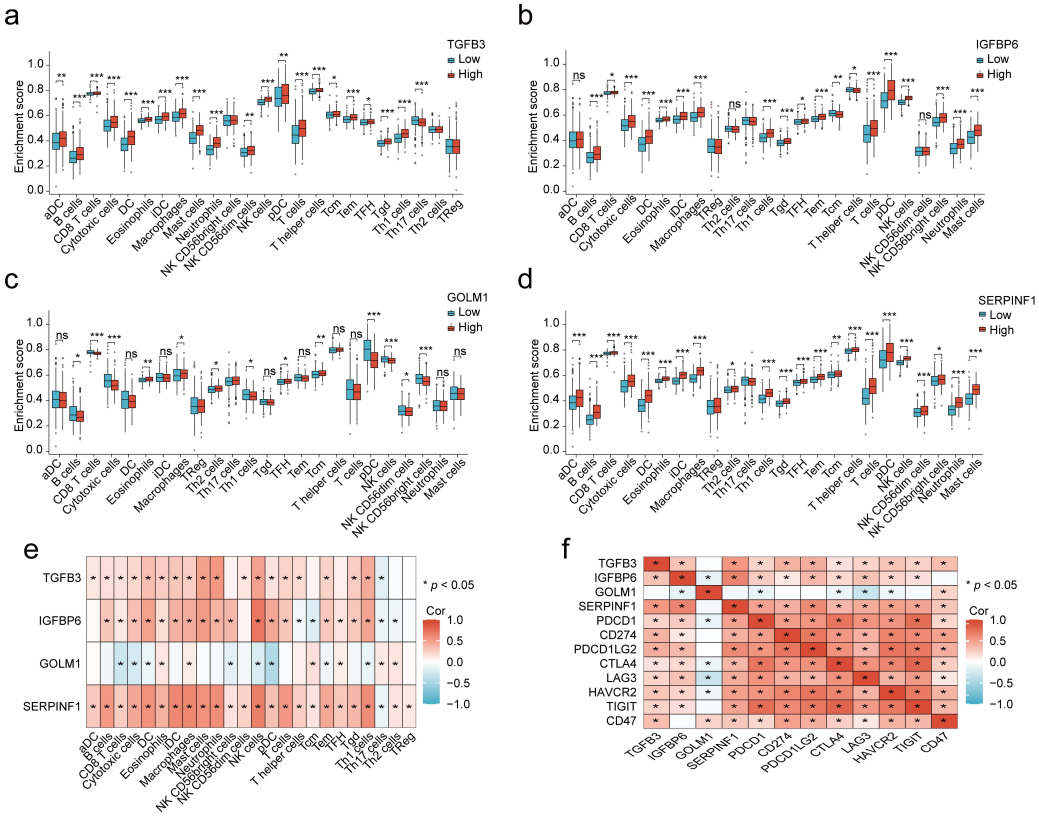

FIGURE 9. Immune microenvironment characteristics of key biomarkers in PCa. Boxplots comparing immune cell enrichment scores between high and low expression groups of (a) TGFB3, (b) IGFBP6, (c) GOLM1, and (d) SERPINF1. (e) Heatmap illustrating the correlation between key biomarkers and immune cell types in the TCGA-PRAD cohort. Positive correlations are shown in red, while negative correlations are shown in blue. (f) Heatmap showing the correlation between key biomarkers and immune checkpoint genes in the TCGA-PRAD cohort. Statistical significance is denoted by *, **, and *** for $p < 0.05$, $p < 0.01$, and $p < 0.001$, respectively.

lations with PDCD1, CTLA4, LAG3, and HAVCR2 (Fig. 9f).

3.10 Network construction and molecular docking with small molecules

To explore potential small molecules capable of targeting key biomarkers, an interaction network was constructed between candidate compounds and target proteins (Fig. 10a). The analysis revealed that several small molecules could simultaneously target two core proteins, such as diethylstilbestrol, irinotecan, 7646-79-9, camptothecin, selenium, and vitamin E. Among these, diethylstilbestrol was identified as interacting with both TGFB3 and IGFBP6 and was selected for molecular docking analysis. The three-dimensional (3D) structures of human TGFB3 (PDB ID: 2PJY) and IGFBP6 (PDB ID: 1RMJ) were obtained for docking analysis. The results demonstrated that diethylstilbestrol binds specifically to the active sites of TGFB3 (Vina score = −5.5) and IGFBP6 (Vina score = −4.6), forming stable complexes (Fig. 10b). These findings highlight diethylstilbestrol as a promising candidate for modulating the activity of TGFB3 and IGFBP6, offering potential therapeutic implications.

4. Discussion

In this study, we systematically investigated potential diagnostic biomarkers and therapeutic targets through analysis of the human plasma proteome. By MR analysis, we identified 66 plasma proteins with significant associations with PCa. Among them, COL3A1 and IL1RL2 exhibited notable associations, suggesting their potential relevance to PCa risk. COL3A1, which encodes type III collagen, may contribute to tumor progression by remodeling the extracellular matrix and promoting cancer cell invasion [36, 37]. Similarly, IL1RL2, a key mediator in inflammatory signaling pathways [38], highlights the potential role of chronic inflammation in PCa development. These findings align with previous evidence linking the tumor microenvironment and inflammation to prostate carcinogenesis. While further studies are needed to validate their roles, COL3A1 and IL1RL2 represent intriguing candidates for future investigation into PCa pathogenesis.

The analysis of bulk RNA-seq data revealed significant differences in gene expression between PCa and normal tissues. To further explore the tumor microenvironment (TME) in PCa, scRNA-seq and spatial transcriptomics (ST) were integrated [39]. Single-cell RNA-seq analysis revealed that immune cells, such as CD4+ and CD8+ T cells, exhibited a more concentrated distribution compared to normal tissues, whereas epithelial and fibroblast cells showed a more dispersed distribution, suggesting the formation of immune niches potentially driven by tumor-secreted chemokines or cytokines [40]. Spatial analysis also identified immune-enriched clusters predominantly in tumor regions, while stromal cell-related clusters were more prominent in normal tissues, indicating significant stromal remodeling during tumorigenesis. This remodeling, likely mediated by cancer-associated fibroblasts (CAFs), may facilitate tumor progression by creating physical

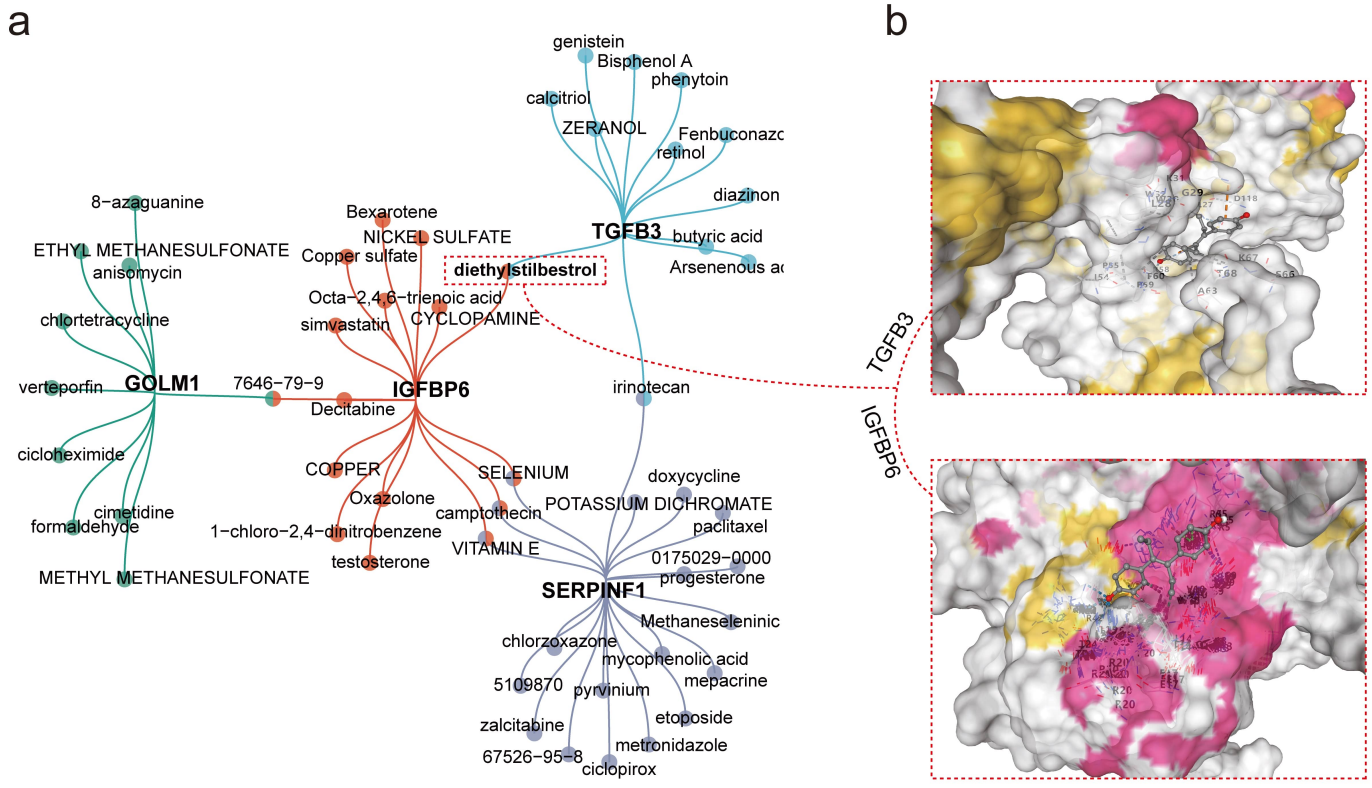

FIGURE 10. Network analysis and molecular docking with small molecules. (a) Interaction network of small molecules and key biomarkers. (b) Molecular docking results of selected small molecules with TGFB3 and IGFBP3. GOLM1, Golgi Membrane Protein 1; TGFB3, Transforming Growth Factor Beta 3; IGFBP6, Insulin-Like Growth Factor Binding Protein 6; SERPINF1, Serpin Family F Member 1.

and biochemical barriers to immune cell infiltration through extracellular matrix modification and the secretion of immunosuppressive factors [41–43]. The identification of immune-enriched and stromal-dominant regions offers valuable insights into the dynamic interactions between immune and stromal cells in PCa, thus providing a foundation for potential strategies to modulate the tumor microenvironment and enhance anti-tumor immunity.

The enrichment analysis for PCa-PP and DEGs highlights key mechanisms driving PCa progression. For PCa-PP, extracellular matrix (ECM)-related terms and inflammatory processes suggest that structural remodeling and immune responses play pivotal roles in facilitating tumor progression [44]. Bulk-DEGs revealed enrichment in metabolic and signaling pathways, such as glutathione metabolism [45] and PI3K-Akt signaling [46], reflecting metabolic shifts and dysregulated cell signaling in PCa. Additionally, glycosaminoglycan binding and epithelial cell proliferation highlight the interplay between ECM and tumor growth [47]. ST-DEGs further emphasized immune modulation and ECM organization, particularly through complement cascades and cell adhesion molecules, revealing spatial heterogeneity within the tumor microenvironment. These findings collectively underscore the importance of ECM dynamics, immune interactions, and metabolic alterations in PCa pathogenesis, suggesting that targeting these processes may provide new therapeutic opportunities, particularly in addressing tumor heterogeneity and microenvironmental complexity.

We further performed an integrated analysis of PCa-PP and DEGs and identified four key biomarkers associated with PCa. Combining these multi-omics approaches with MR analysis allows for the identification of causal plasma proteins with significantly altered gene expression levels in PCa, providing a comprehensive understanding of their roles in tumorigenesis. TGFB3 plays a complex, context-dependent role in cancer biology, being linked to tumorigenesis in some contexts while also exhibiting tumor-suppressive effects, such as maintaining tissue homeostasis and suppressing early-stage tumors [48]. Studies show that TGFB3 expression is typically reduced in PCa tissues, particularly in basal epithelial cells, which may promote tumor progression. IGFBP6, known for modulating insulin-like growth factor (IGF) signaling, also plays dual roles in tumor. It can suppress tumor growth by inhibiting IGF activity but can also promote metastasis, especially in advanced PCa, through effects on the tumor microenvironment or cell migration [49]. GOLM1 is a Golgi membrane protein and has been widely studied for its pro-tumor role in PCa. Its overexpression is closely associated with increased tumor cell invasiveness and metastatic potential, possibly by facilitating the secretion and transport of tumor-related proteins [50]. SERPINF1, as a serine protease inhibitor, is closely associated with ECM remodeling in PCa. SERPINF1 may exert tumor-suppressive effects by maintaining ECM integrity and inhibiting angiogenesis, thereby limiting tumor invasion and metastasis [51].

Spatial visualization further confirmed their expression patterns. TGFB3, IGFBP6, and SERPINF1 exhibited higher expression in normal prostate regions, while GOLM1 showed increased expression in PCa regions, highlighting their potential roles in tumorigenesis. These spatial patterns provide valuable insights into the distinct functional roles of these factors within the tumor microenvironment. The diagnostic potential of these key biomarkers was evaluated by ROC curve analysis, which demonstrated their robust diagnostic performance. Functional enrichment analysis revealed that these factors are involved in pathways such as SMAD signaling, cytokine binding, and Wnt signaling, underscoring their critical roles in PCa progression. Collectively, these findings highlight the potential of TGFB3, IGFBP6, GOLM1, and SERPINF1 as diagnostic biomarkers or therapeutic targets in PCa.

The results of immune microenvironment characteristics of key biomarkers indicate that TGFB3, IGFBP6, and SERPINF1 may enhance immune cell infiltration and immune activation, potentially contributing to anti-tumor immunity. Conversely, GOLM1 appears to suppress immune infiltration and may play a role in creating an immunosuppressive tumor microenvironment. The strong positive correlations of TGFB3, IGFBP6, and SERPINF1 with immune checkpoint molecules suggest their potential as biomarkers or therapeutic targets in immunotherapy. On the other hand, the immunosuppressive role of GOLM1 highlights its potential as a target for reversing immune evasion. These findings provide a foundation for further exploration of the roles of these key biomarkers in tumor immunity and their application in immunotherapeutic strategies.

Diethylstilbestrol, an androgen receptor antagonist, effectively inhibits androgen signaling in hormone-dependent cancers such as prostate cancer [52]. Molecular docking revealed its ability to specifically bind TGFB3 and IGFBP6 with favorable affinities, forming stable complexes. TGFB3, a key immunosuppressive factor in the tumor microenvironment, promotes immune evasion, and its inhibition by diethylstilbestrol may enhance T-cell activation and anti-tumor immune responses. IGFBP6, involved in regulating cell growth and differentiation, may further suppress tumor progression when modulated. This dual mechanism of action highlights the therapeutic potential of diethylstilbestrol, as it not only directly inhibits tumor growth but may also improve the tumor immune microenvironment to enhance the efficacy of immunotherapy. By targeting TGFB3, it offers a rationale for combination strategies with immune checkpoint inhibitors, particularly in patients resistant to conventional androgen deprivation therapy. Future studies should focus on validating its immunomodulatory effects and evaluating its potential in combination treatments to develop more effective strategies for advanced prostate cancer.

However, several limitations remain in this study. First, while our study benefits from a multi-omics approach, the sample sizes for certain datasets, such as scRNA-seq, were limited. For instance, the scRNA-seq analysis was based on only four tumor samples, which may not fully capture the cellular heterogeneity in the broader prostate cancer population. Second, our analysis did not extend to correlating the identified biomarkers with established clinicopathological features like the Gleason score or with TCGA's defined molecular subtypes (*e.g.*, E26 transformation-specific transcription factor related gene (ERG)-fusion status). While our findings on the immune microenvironment provide a strong indication of their

relevance to tumor heterogeneity, a direct analysis of these other features is a critical next step to fully understand their prognostic and predictive utility. Third, the functional roles of the biomarkers and the efficacy of potential small-molecule drugs require experimental validation through *in vitro* and *in vivo* studies, and the clinical applicability of our diagnostic model, despite its high accuracy *in silico*, must be validated in prospective clinical cohorts. Future research will focus on addressing these limitations to advance our findings towards clinical translation.

In conclusion, this study integrates MR analysis with multi-omics approaches to identify key biomarkers associated with PCa. By revealing the dynamic characteristics of the tumor microenvironment and its role in PCa progression, this work provides novel insights into the molecular mechanisms of PCa. While further validation is needed, these findings contribute to the development of more precise diagnostic and therapeutic strategies.

5. Conclusions

Integrating Mendelian randomization and multi-omics, we identified TGFB3, IGFBP6, GOLM1, and SERPINF1 as pivotal plasma biomarkers for prostate cancer, implicated in extracellular matrix and immune pathways. A diagnostic model combining these proteins showed high accuracy (AUC = 0.911), while diethylstilbestrol emerged as a promising therapeutic candidate. These insights highlight actionable targets for diagnosis and therapy, requiring further clinical validation.

ABBREVIATIONS

AUC, area under the curve; BP, biological processes; bulk RNA-seq, bulk RNA sequencing; CAFs, cancer-associated fibroblasts; CC, cellular components; CD, cluster of differentiation; COL3A1, collagen type III alpha 1 chain; DsigDB, drug signature database; ECM, extracellular matrix; ERG, E26 transformation-specific transcription factor related gene; GEO, Gene Expression Omnibus; GO, Gene Ontology; GSVA, gene set variation analysis; GWAS, genome-wide association study; IGF, insulin-like growth factor; IGFBP6, insulin-like growth factor binding protein 6; IL1RL2, interleukin 1 receptor like 2; IVW, inverse variance-weighted; IVs, instrumental variables; KEGG, Kyoto Encyclopedia of Genes and Genomes; LD, linkage disequilibrium; logFC, logarithm of fold change; MIA, multiple intercellular analysis; MF, molecular functions; MR, Mendelian randomization; PCA, principal component analysis; PCa, prostate cancer; PCa-PP, prostate cancer-associated plasma proteins; PI3K-Akt, phosphoinositide 3-kinase-protein kinase B pathway; PDB, protein data bank; PPI, protein-protein interaction; PRESSO, pleiotropy residual sum and outlier; PRAD, prostate adenocarcinoma; ROC, receiver operating characteristic; SCTransform, single-cell transform; SD, standard deviation; SNE, stochastic neighbor embedding; SNN, shared nearest neighbor; SingleR, single-cell recognition; SMAD, mothers against decapentaplegic homolog; ST, spatial transcriptomics; TCGA, The Cancer Genome Atlas; TGFB3, transforming growth factor beta 3; TME, tumor microenvironment; UMAP, uniform manifold approximation and projection; VST, variance-stabilizing transformation; Wnt, Wingless-related integration site; 3D, three-dimensional.

AVAILABILITY OF DATA AND MATERIALS

The pQTL data were obtained from the publicly available deCODE genetics repository, which permits use for academic research. All data pertinent to this study are contained within the article or can be obtained from the corresponding author upon a reasonable request.

AUTHOR CONTRIBUTIONS

HX and QL—participated in the design, interpretation of the study, and review of the manuscript. Both authors contributed to data acquisition, performed statistical analyses, provided technical support, drafted the manuscript, offered critical comments and suggestions, and revised the manuscript. Additionally, both authors were involved in funding support. The final manuscript was read and approved by both authors.

ETHICS APPROVAL AND CONSENT TO PARTICIPATE

Not applicable.

ACKNOWLEDGMENT

Both authors express their gratitude to the generous contributors of the GEO database.

FUNDING

This research received no external funding.

CONFLICT OF INTEREST

The authors declare no conflict of interest.

SUPPLEMENTARY MATERIAL

Supplementary material associated with this article can be found, in the online version, at https://oss.jomh.org/files/article/20602899232046940 16/attachment/Supplementary%20material.zip.

REFERENCES

[1] Wasim S, Lee SY, Kim J. Complexities of prostate cancer. International Journal of Molecular Sciences. 2022; 23: 14257.

[2] Zhang X, Yang L, Liu S, Cao LL, Wang N, Li HC, *et al*. Interpretation on the report of global cancer statistics 2022. Chinese Journal of Oncology. 2024; 46: 710–721. (In Chinese)

[3] Yao B, Zhu S, Wei X, Chen MK, Feng Y, Li Z, *et al*. The circSPON2/miR-331-3p axis regulates PRMT5, an epigenetic regulator of CAMK2N1 transcription and prostate cancer progression. Molecular Cancer. 2022; 21: 119.

[4] Papier K, Atkins JR, Tong TYN, Gaitskell K, Desai T, Ogamba CF, *et al*. Identifying proteomic risk factors for cancer using prospective and exome analyses of 1463 circulating proteins and risk of 19 cancers in the UK Biobank. Nature Communications. 2024; 15: 401.

[5] Davies MPA, Sato T, Ashoor H, Hou L, Liloglou T, Yang R, *et al*. Plasma protein biomarkers for early prediction of lung cancer. eBioMedicine. 2023; 93: 104686.

[6] Magnusson MI, Agnarsson BA, Jonasson JG, Tryggvason T, Aeffner F, le Roux L, *et al*. Histopathology and levels of proteins in plasma associate with survival after colorectal cancer diagnosis. British Journal of Cancer. 2023; 129: 1142–1151.

[7] Hsieh CH, Wang YC. Emerging roles of plasma gelsolin in tumorigenesis and modulating the tumor microenvironment. The Kaohsiung Journal of Medical Sciences. 2022; 38: 819–825.

[8] Bidoki NH, Zera KA, Nassar H, Drag LL, Mlynash M, Osborn E, *et al*. Machine learning models of plasma proteomic data predict mood in chronic stroke and tie it to aberrant peripheral immune responses. Brain, Behavior, and Immunity. 2023; 114: 144–153.

[9] Huang C, Wang Y, Lin X, Chan TF, Lai KP, Li R. Uncovering the functions of plasma proteins in ulcerative colitis and identifying biomarkers for BPA-induced severe ulcerative colitis: a plasma proteome analysis. Ecotoxicology and Environmental Safety. 2022; 242: 113897.

[10] Birney E. Mendelian randomization. Cold Spring Harbor Perspectives in Medicine. 2022; 12: a041302.

[11] Chen C, Wang J, Pan D, Wang X, Xu Y, Yan J, *et al*. Applications of multi-omics analysis in human diseases. MedComm. 2023; 4: e315.

[12] Baysoy A, Bai Z, Satija R, Fan R. The technological landscape and applications of single-cell multi-omics. Nature Reviews Molecular Cell Biology. 2023; 24: 695–713.

[13] Tan Z, Chen X, Zuo J, Fu S, Wang H, Wang J. Comprehensive analysis of scRNA-Seq and bulk RNA-Seq reveals dynamic changes in the tumor immune microenvironment of bladder cancer and establishes a prognostic model. Journal of Translational Medicine. 2023; 21: 223.

[14] Hsieh WC, Budiarto BR, Wang YF, Lin CY, Gwo MC, So DK, *et al*. Spatial multi-omics analyses of the tumor immune microenvironment. Journal of Biomedical Science. 2022; 29: 96.

[15] Eldjarn GH, Ferkingstad E, Lund SH, Helgason H, Magnusson OT, Gunnarsdottir K, *et al*. Large-scale plasma proteomics comparisons through genetics and disease associations. Nature. 2023; 622: 348–358.

[16] Mounier N, Kutalik Z. Bias correction for inverse variance weighting Mendelian randomization. Genetic Epidemiology. 2023; 47: 314–331.

[17] Bowden J, Davey Smith G, Burgess S. Mendelian randomization with invalid instruments: effect estimation and bias detection through Egger regression. International Journal of Epidemiology. 2015; 44: 512–525.

[18] Hemani G, Zheng J, Elsworth B, Wade KH, Haberland V, Baird D, *et al*. The MR-Base platform supports systematic causal inference across the human phenome. eLife. 2018; 7: e34408.

[19] Verbanck M, Chen CY, Neale B, Do R. Detection of widespread horizontal pleiotropy in causal relationships inferred from Mendelian randomization between complex traits and diseases. Nature Genetics. 2018; 50: 693–698.

[20] Burgess S, Thompson SG. Interpreting findings from Mendelian randomization using the MR-Egger method. European Journal of Epidemiology. 2017; 32: 377–389.

[21] Huedo-Medina TB, Sánchez-Meca J, Marín-Martínez F, Botella J. Assessing heterogeneity in meta-analysis: Q statistic or I2 index? Psychological Methods. 2006; 11: 193–206.

[22] Ritchie ME, Phipson B, Wu D, Hu Y, Law CW, Shi W, *et al*. Limma powers differential expression analyses for RNA-sequencing and microarray studies. Nucleic Acids Research. 2015; 43: e47.

[23] Wickham H. ggplot2: elegant graphics for data analysis. 2nd edn. Springer: Cham. 2016.

[24] Kolde R. pheatmap: Pretty Heatmaps, R package version 1.0.13. 2025. Available at: https://github.com/raivokolde/pheatmap (Accessed: 13 April 2026).

[25] Slovin S, Carissimo A, Panariello F, Grimaldi A, Bouché V, Gambardella G, *et al*. Single-cell RNA sequencing analysis: a step-by-step overview. Methods in Molecular Biology. 2021; 2284: 343–365.

[26] Aran D, Looney AP, Liu L, Wu E, Fong V, Hsu A, *et al*. Reference-based analysis of lung single-cell sequencing reveals a transitional profibrotic macrophage. Nature Immunology. 2019; 20: 163–172.

[27] Chen TY, You L, Hardillo JAU, Chien MP. Spatial transcriptomic technologies. Cells. 2023; 12: 2042.

[28] Yu G, Wang LG, Yan GR, He QY. Dose: an R/Bioconductor package for disease ontology semantic and enrichment analysis. Bioinformatics. 2015; 31: 608–609.

[29] Yu G, Wang LG, Han Y, He QY. clusterProfiler: an R package for comparing biological themes among gene clusters. Omics. 2012; 16: 284–287.

[30] Franz M, Rodriguez H, Lopes C, Zuberi K, Montojo J, Bader GD, *et al*. GeneMANIA update 2018. Nucleic Acids Research. 2018; 46: W60–W64.

[31] Hänzelmann S, Castelo R, Guinney J. GSVA: gene set variation analysis for microarray and RNA-seq data. BMC Bioinformatics. 2013; 14: 7.

[32] Yoo M, Shin J, Kim J, Ryall KA, Lee K, Lee S, *et al*. DSigDB: drug signatures database for gene set analysis. Bioinformatics. 2015; 31: 3069–3071.

[33] Jo S, Im W. Glycan fragment database: a database of PDB-based glycan 3D structures. Nucleic Acids Research. 2013; 41: D470–D474.

[34] Wang Y, Xiao J, Suzek TO, Zhang J, Wang J, Zhou Z, *et al*. PubChem's BioAssay database. Nucleic Acids Research. 2012; 40: D400–D412.

[35] Liu Y, Yang X, Gan J, Chen S, Xiao ZX, Cao Y. CB-Dock2: improved protein-ligand blind docking by integrating cavity detection, docking and homologous template fitting. Nucleic Acids Research. 2022; 50: W159–W164.

[36] Kuivaniemi H, Tromp G. Type III collagen (COL3A1): gene and protein structure, tissue distribution, and associated diseases. Gene. 2019; 707: 151–171.

[37] Van Espen B, Oo HZ, Collins C, Fazli L, Molinolo A, Yip K, *et al*. RNF185 control of COL3A1 expression limits prostate cancer migration and metastatic potential. Molecular Cancer Research. 2024; 22: 41–54.

[38] Tomuschat C, O'Donnell AM, Coyle D, Puri P. Altered expression of IL36γ and IL36 receptor (IL1RL2) in the colon of patients with Hirschsprung's disease. Pediatric Surgery International. 2017; 33: 181–186.

[39] Lee CYC, McCaffrey J, McGovern D, Clatworthy MR. Profiling immune cell tissue niches in the spatial-omics era. The Journal of Allergy and Clinical Immunology. 2025; 155: 663–677.

[40] Codrici E, Enciu AM, Popescu ID, Mihai S, Tanase C. Glioma stem cells and their microenvironments: providers of challenging therapeutic targets. Stem Cells International. 2016; 2016: 5728438.

[41] Ma C, Yang C, Peng A, Sun T, Ji X, Mi J, *et al*. Pan-cancer spatially resolved single-cell analysis reveals the crosstalk between cancer-associated fibroblasts and tumor microenvironment. Molecular Cancer. 2023; 22: 170.

[42] Mao X, Xu J, Wang W, Liang C, Hua J, Liu J, *et al*. Crosstalk between cancer-associated fibroblasts and immune cells in the tumor microenvironment: new findings and future perspectives. Molecular Cancer. 2021; 20: 131.

[43] Wu F, Yang J, Liu J, Wang Y, Mu J, Zeng Q, *et al*. Signaling pathways in cancer-associated fibroblasts and targeted therapy for cancer. Signal Transduction and Targeted Therapy. 2021; 6: 218.

[44] Han X, Caron JM, Brooks PC. Cryptic collagen elements as signaling hubs in the regulation of tumor growth and metastasis. Journal of Cellular Physiology. 2020; 235: 9005–9020.

[45] Bansal A, Simon MC. Glutathione metabolism in cancer progression and treatment resistance. Journal of Cell Biology. 2018; 217: 2291–2298.

[46] Chen H, Zhou L, Wu X, Li R, Wen J, Sha J, *et al*. The PI3K/AKT pathway in the pathogenesis of prostate cancer. Frontiers in Bioscience. 2016; 21: 1084–1091.

[47] Dang T, Liou GY. Macrophage cytokines enhance cell proliferation of normal prostate epithelial cells through activation of ERK and Akt. Scientific Reports. 2018; 8: 7718.

[48] Wang L, Guan X, Hu Q, Wu Z, Chen W, Song L, *et al*. TGFB3 downregulation causing chordomagenesis and its tumor suppression role maintained by Smad7. Carcinogenesis. 2021; 42: 913–923.

[49] Koike H, Ito K, Takezawa Y, Oyama T, Yamanaka H, Suzuki K. Insulin-like growth factor binding protein-6 inhibits prostate cancer cell proliferation: implication for anticancer effect of diethylstilbestrol in hormone refractory prostate cancer. British Journal of Cancer. 2005; 92:

1538–1544.

[50] Yan G, Ru Y, Wu K, Yan F, Wang Q, Wang J, *et al*. GOLM1 promotes prostate cancer progression through activating PI3K-AKT-mTOR signaling. Prostate. 2018; 78: 166–177.

[51] Xu B, Li J, Liu X, Li C, Chang X. TXNDC5 is a cervical tumor susceptibility gene that stimulates cell migration, vasculogenic mimicry and angiogenesis by down-regulating SERPINF1 and TRAF1 expression. Oncotarget. 2017; 8: 91009–91024.

[52] Bigot P, Mouzat K, Lebdai S, Bahut M, Benhabiles N, Tassin GC, *et al*. Quantitative proteomic determination of diethylstilbestrol action on prostate cancer. Asian Journal of Andrology. 2013; 15: 413–420.

How to cite this article: Hua Xiang, Qian Liu. Plasma proteome-based integrated mendelian randomization and multi-omics analysis identifies potential diagnostic biomarkers and therapeutic targets for prostate cancer. Journal of Men's Health. 2026; 22(5): 66-80. doi: 10.22514/jomh.2026.042.